

# A high-resolution magnetic tweezer for single-molecule measurements

Kipom Kim<sup>1</sup> and Omar A. Saleh<sup>1,2,\*</sup>

<sup>1</sup>Materials Department and <sup>2</sup>Biomolecular Science and Engineering Program, University of California, Santa Barbara, CA 93106, USA

Received May 1, 2009; Revised July 26, 2009; Accepted August 17, 2009

## ABSTRACT

**Magnetic tweezers (MT) are single-molecule manipulation instruments that utilize a magnetic field to apply force to a biomolecule-tethered magnetic bead while using optical bead tracking to measure the biomolecule's extension. While relatively simple to set up, prior MT implementations have lacked the resolution necessary to observe sub-nanometer biomolecular configuration changes. Here, we demonstrate a reflection-interference technique for bead tracking, and show that it has much better resolution than traditional diffraction-based systems. We enhance the resolution by fabricating optical coatings on all reflecting surfaces that optimize the intensity and contrast of the interference image, and we implement feedback control of the focal position to remove drift. To test the system, we measure the length change of a DNA hairpin as it undergoes a folding/unfolding transition.**

## INTRODUCTION

Over the past 10 years, a variety of experimental techniques have been developed that allow the mechanical manipulation of a single biological molecule and the sensing of its interactions with other biomolecules (1–3). These single-molecule measurements are extraordinarily sensitive, as they are capable of applying piconewton-scale forces and measuring displacements of nanometers, allowing them to provide direct data on the molecular-scale workings of biological systems. Importantly, these data are quantitative, and can thus be directly compared to other information, such as crystallographic structures or biochemical / biophysical theories, in order to attain a complete understanding of biomolecular behavior.

The magnetic tweezer (MT) is a simple and stable tool to stretch and twist biomolecules and to measure their extension over time (4–8). It is based on the manipulation, using magnetic fields, of a paramagnetic bead (1–5  $\mu\text{m}$  in

diameter) that is tethered to a glass surface through a single biomolecule. The field applies a force to the bead that stretches or twists the molecule. In a typical experiment, a physical change to the tethered biomolecule causes its extension to increase or decrease, raising or lowering the vertical position of the bead. Traditionally, bead height is measured by analyzing the bead's diffraction image when viewed in a transmitted light geometry (9,10). Thus, the MT's capability to measure physical changes to the biomolecule depends on the ability to relate variations in the diffraction image to the position of the bead.

The resolution of any single-molecule technique is impaired by two sources of noise: the Brownian motion of the bead, which can be reduced by using small beads, high forces, and short tethers, and the intrinsic resolution of the instrument, which depends on the sensing technique utilized and the instrument's stability. In typical diffraction-based MT setups, the intrinsic resolution is limited to  $\sim 1\text{ nm}$  (10), which suffers in comparison to high-resolution optical tweezer methods (11). This low-resolution originates from the relatively small lateral motion of the diffraction interference fringes with bead height. Limited resolution is acceptable in the low-force regime, where Brownian motion of the tethered bead dominates the experimental noise. However, when using high forces, Brownian motion is reduced and the intrinsic resolution becomes limiting.

To overcome this limit, we have adapted Reflection Interference Contrast Microscopy (RICM) to the MT. In RICM, objective-side illumination creates an interference pattern between rays reflecting from a glass surface and those reflecting from an object in solution located near to the surface (12,13). Bead height is calculated by comparing the measured interference pattern to a theoretical model that predicts the fringe shape based on the optical geometry (13). Importantly, the interference fringes from RICM have a much larger variation with bead height than those from diffraction. Indeed, prior applications of RICM have indicated sub-nanometer accuracy in measured bead height is possible (14,15).

\*To whom correspondence should be addressed. Tel: +1 805 893 8814; Fax: +1 805 893 8486; Email: saleh@engineering.ucsb.edu

There are two difficulties in using RICM with an MT. First, the optical properties are not ideal: both the magnetic beads and the glass surface have a similar refractive index as the surrounding solution. Without a significant difference in refractive index, little light would be reflected from each interface, allowing background illumination (stemming from, e.g. internal reflections within the bead) to obscure the RICM interferogram. Thus, it is necessary to adjust the properties of each surface both to achieve optimal interferogram intensity and contrast and to cut-off background light. Second, to accurately model and analyze the RICM interference pattern, the image plane of the microscope must be stably maintained at a known, fixed position—in particular, at the glass-water interface. Thus, it is necessary to minimize the defocusing effects of thermal and mechanical drift. We overcame these difficulties by, respectively, fabricating optical coatings on all reflecting surfaces that optimize the intensity and contrast of the interference image, and implementing feedback control of the focal position to remove drift.

## MATERIALS AND METHODS

### Materials

**DNA samples.** DNA constructs with a single hairpin were based on PAGE-purified DNA oligomers (Integrated DNA Technologies) that have a hairpin sequence, and non-palindromic ligation sequences at each end. The hairpins (S20T8, S30T8) have 20-bp stem and 8-nt Thymine-loop (S20T8) and 30-bp stem and 8-nt Thymine-loop (S30T8), of which stem sequences are GA GTCAACGTCTGGATCCTA and GAGGCGGTCGCC TGCGCACGCTGGCCTCGC, respectively.

The 5'-end of the hairpin was ligated to an 800-bp dsDNA handle with a 14-nt complementary overhang at one end and a digoxigenin label at the other end, while the 3'-end of the hairpin was annealed to a 15-nt oligomer (Integrated DNA Technologies) with a 5' biotin label. The dsDNA handle (800 bp) was prepared by means of Autosticky PCR using Lambda-phage DNA (New England Biolabs N3011) as the template, one 5' digoxigenin-labeled primer (MWG Biotech), and one primer with a 15-nt extension after a deoxyribose spacer site (Integrated DNA Technologies) to achieve the specified dsDNA length and 5'-end (16). A 1738-bp double-stranded DNA without a hairpin was prepared by means of PCR using Lambda-phage DNA as the template, and primers containing, respectively, 5' digoxigenin and 5' biotin labels (MWG Biotech).

**Beads.** Magnetic beads of 2.8  $\mu\text{m}$  diameter (Invitrogen Dynal-M280) were used for the diffraction measurements and 4.5  $\mu\text{m}$ -diameter magnetic beads (Invitrogen Dynal-M450) were used for the RICM measurements. Dynal M450 beads have 5% polydispersity in diameter. Our simulation (see below) indicates that a 5% polydispersity affects the measured bead height by <3%; direct measurement of the individual tethered bead's diameter would reduce this error. One micrometer-diameter

polystyrene beads (Bangs Laboratories PS04N) were used as reference objects stuck on the coverglass.

### Optical enhancement of reflecting surfaces

To enhance each surface's optical characteristics for RICM, both the magnetic bead and the glass surface were coated with nanofabricated thin layers (Figure 1). To make beads with a half gold surface, the solution of magnetic beads was dried on a flat solid surface. The surface was coated sequentially with Ti (5 nm) and Au (50 nm) using electron-beam metal evaporation; the Ti layer acts as an adhesion layer between the polystyrene of the bead and the gold. Half-coated beads were resuspended in phosphate-buffered saline using sonication, and purified by magnetic separation. Separately, the glass substrate was sequentially coated with TiO<sub>2</sub> (50 nm,  $n = 2.5$ ) and SiO<sub>2</sub> (25 nm,  $n = 1.42$ ) using electron-beam dielectric evaporation. The coatings were fabricated in the UCSB Nanofabrication Facility using Temescal electron-beam evaporators.

### Immobilization of DNA

The magnetic bead's gold-coated surface was biotinylated by incubating overnight in a biotinylation reagent (0.2% w/v Sulfo-NHS-SS-Biotin in Phosphate-buffered saline, pH 7.4): the Sulfo-NHS-SS-Biotin (Pierce Ez-Link) was used after reducing the disulfide bond with TCEP (Sigma). The biotinylated gold surface was then coated with streptavidin (Roche Diagnostics). The coverglass's SiO<sub>2</sub> surface was coated with an anti-digoxigenin antibody (Roche Diagnostics) through non-specific adsorption.

In both the diffraction and RICM measurements, the biotin and digoxigenin labels on the DNA were bound, respectively, to the streptavidin on the magnetic bead and the anti-digoxigenin on the coverglass (Figure 1a).

### Magnetic tweezer (MT)

The basic MT system is shown in Figure 2. We used an inverted microscope (Nikon TE2000-U) with an oil-immersion objective (Nikon Plan APO 1.4 NA 100 $\times$ ). The applied magnetic field is generated by a pair of permanent (NdFeB) magnets (12.5 mm cubes, DuraMag NS-505050) located above the sample stage, separated by 1 mm, and with their magnetic moments aligned anti-parallel to each other. Variation of the field in the sample plane is achieved by translating the magnets with a DC servo motor (Physik Instrumente M-126.PD1) in the range between 1 and 25 mm from the stage. Magnetic beads can be rotated about the illumination axis by rotating the magnet pair with a DC servo motor (Physik Instrumente C-150.PD); we use the trajectory of rotated beads to exclude mis-tethered beads (17).

We calibrate the force applied to magnetic beads by analyzing the power spectrum of measured lateral fluctuations, as is standard for such techniques (9). Based on that analysis, we estimate the uncertainty in the measured force to be 10%.

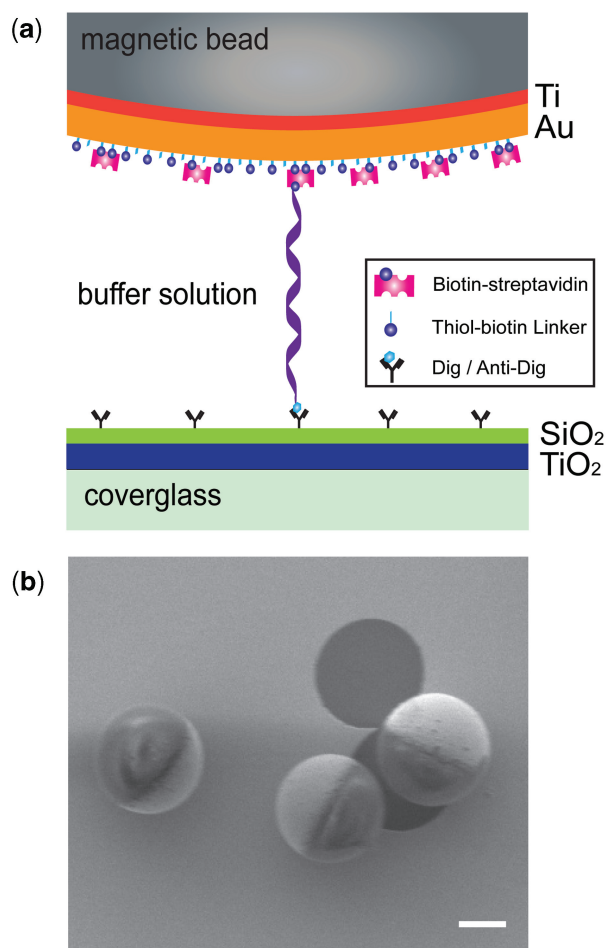


**Figure 1.** (a) Schematic diagram of optical and biochemical coatings. (b) Electron micrograph of 4.5  $\mu\text{m}$  diameter gold-coated beads; the bright half of each bead is the gold-coated surface. Scale bar: 2  $\mu\text{m}$ .

### Illumination, imaging and tracking

Detail of the illumination scheme and stabilizing method were as explained in Ref. (10,15). Briefly, there are separate light sources to make the diffraction and interference image of the beads (Figure 2). A monochromatic incident beam (red) from an LED enters through the gap between the magnets and creates a diffraction pattern of the bead on the image plane. A second monochromatic beam for RICM (green) uniformly illuminates the image plane by focusing the incident beam on the back focal plane of the objective lens; the smallest achievable illumination numerical aperture (INA) is 0.48. The images were then acquired with a CCD camera (JAI CV-A10CL), which has 60 Hz frame rate and 3.3  $\mu\text{s}$  minimum exposure. From each acquired image, lateral center positions and height ( $x$ ,  $y$ ,  $h$ ) and radial averaged intensity profiles of the interference image  $I(r)$  of magnetic beads were calculated and stored in real time using custom written tracking software. In the diffraction method,  $h$  was calculated in real-time from previously-acquired calibration images. In RICM,  $h$  was estimated in real-time by scaling the radius of the first interference

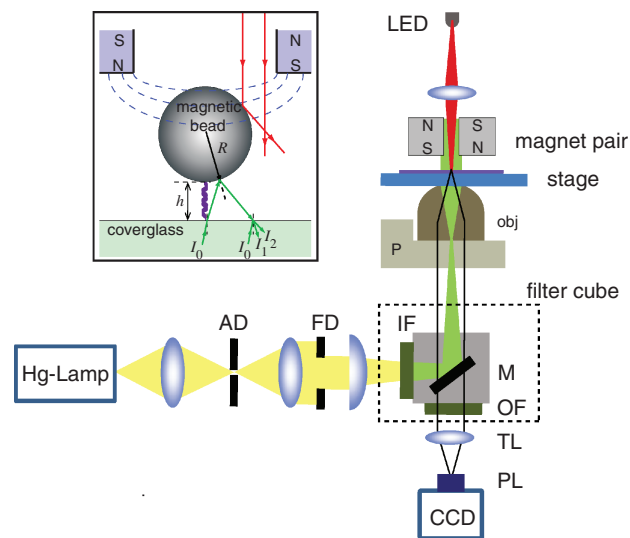


**Figure 2.** Schematic diagram of the experimental setup. AD: aperture diaphragm, FD: field diaphragm, IF: incident bandpass filter, OF: imaging bandpass filter, TL: tube lens, PL: parfocal lens, M: beam splitter, P: piezo objective positioner, Obj: objective lens. CCD is a CCD camera with 60 Hz frame rate. The inset shows the geometry of both the tethered bead and the transmitted and reflected beams.

ring with a sensitivity factor pre-estimated numerically for each bead. After completing the experiments,  $h$  values for RICM were re-calculated from the stored  $I(r)$  using custom written analysis software. The illumination and the imaging method are chosen by switching the filter block and the tracking-software.

The piezo objective positioner (Mad City Labs F-100) on which the objective lens is mounted was used to implement feedback control of the focal position for RICM, and to make the calibration image for the diffraction method; it has 0.2 nm spatial resolution, 20 ms time response and a 100  $\mu\text{m}$  travel range.

### RICM re-analysis

In RICM-based measurements, all  $h$  values were re-calculated from the stored  $I(r)$  after finishing an experiment. Each acquired intensity profile  $I(r)$  was compared with a series of intensity profiles  $I_S(r, h)$  simulated based on Ref. (13); simulated profiles were calculated for every 1 nm change in bead height. The absolute squared differences  $\chi^2(h)$  for pairs of  $I(r)$  and  $I_S(r, h)$  were calculated, and the final value of  $h$  was selected by interpolation in the vicinity of the minimum  $\chi^2(h)$ . Details of simulation methods and parameters of RICM-intensity profiles are discussed in the Supplementary Data.

### Stabilization for RICM-based measurements

Low-frequency drift from the apparatus restricts the low-frequency limit on measurable transition rates. To minimize defocusing due to the low-frequency drift, we implemented an active stabilizing method that uses image-analysis-based feedback control of the focal position through piezo-driven motion of the objective



lens (15), where the feedback control automatically adjusted the objective position every 1 s. As shown in our prior work, this feedback method decreased the drift-induced apparent fluctuations in bead height to a standard deviation of 0.12 nm (at a 60 Hz frame rate) and was stable over tens of minutes.

The high-frequency limit on measurable transition rates is set by the time-response of the bead (e.g. how fast can the bead move after a step-like change in tether extension), or by the frame rate of the camera (16 ms), whichever is less. Here, due to the high forces and short tethers used, the frame rate of the camera is the limiting parameter.

## RESULTS AND DISCUSSION

### Effect of optical coating

To optimize the quality of the interference image, we coated the magnetic bead and the glass surface with nano-fabricated layers that enhance each surface's optical characteristics (Figure 1). The gold-coated surface of the magnetic bead increased the reflectance to 80% and completely removed background light from internal reflections within the bead. A further advantage of the gold coating was that it retains biochemical functionality through thiol chemistry. A high refractive index  $\text{TiO}_2$  layer on the coverglass increased the reflectance of that surface, while the  $\text{SiO}_2$  capping layer enabled biochemical functionality. In combination, the gold and dielectric coatings increased the interference pattern's intensity 16-fold and its contrast by 60% (Figure 3). As result of these improvements, we can apply RICM based tracking for bead heights up to 1  $\mu\text{m}$ , corresponding to 3 kbp dsDNA tethers.

### Comparison with traditional method

To evaluate our RICM-based method and to compare it to the traditional diffraction-based method, we performed MT measurements of the force-induced folding/unfolding transition of a DNA hairpin structure (Figure 4a) (18). Figure 5 and Supplementary Figure S1 show that the hairpins repeatedly fold and unfold at a constant applied

force near the critical force. The critical forces are  $10 \pm 1$  pN for S20T8 and  $12 \pm 1$  pN for S30T8. Based on the hairpin length and the elasticity of ssDNA (19), the expected changes in extension for the folding transition are  $17.4 \pm 0.8$  nm for S20T8 and  $27.8 \pm 0.6$  nm for S30T8.

**Sensitivity comparison.** We tested the relative sensitivity of the two approaches by comparing the radial intensity profiles from diffraction to those from RICM for two bead heights, corresponding to the open and closed state of the DNA hairpin S20T8 (Figure 4b and c). For the same change in bead height, the RICM fringes varied much more than the diffraction fringes, indicating the intrinsically higher sensitivity of the RICM-based method. In particular, the first diffraction fringe shifted by 3.8 nm in the sample plane, while the first RICM fringe shifted by 62 nm (Figure 4d and e). Thus, our RICM strategy provides roughly a 16-fold improvement in instrumental resolution. Given the  $\sim 1$  nm intrinsic resolution of diffraction (10), we expect the RICM-based MT will have an intrinsic resolution well below 1 nm.

**Accuracy calibration.** The diffraction-based measurement, while less precise, has the virtue of relying on an accurate experimental calibration scheme that relates bead height to fringe motion (9). In contrast, calibration of the RICM fringes relies on a theoretical model (13). To experimentally verify the accuracy of the model, we compared the diffraction- and RICM-measured extension difference between the folded and unfolded states of the hairpins (Figure 5 and Supplementary Figure S1). Figure 5 shows diffraction- and RICM-measured time traces and height distributions for beads tethered by hairpin S20T8 stretched near its critical force (similar data on hairpin S30T8 is included in the Supplementary Figure S1). For S20T8, the measured changes in extension are  $17.5 \pm 0.2$  nm for diffraction and  $17.4 \pm 0.2$  nm for RICM, while for S30T8, they are  $27.6 \pm 0.1$  nm for diffraction and  $27.4 \pm 0.2$  nm for RICM. Thus, within the experimental error, the results are in agreement both with each other and with the expected extension change,

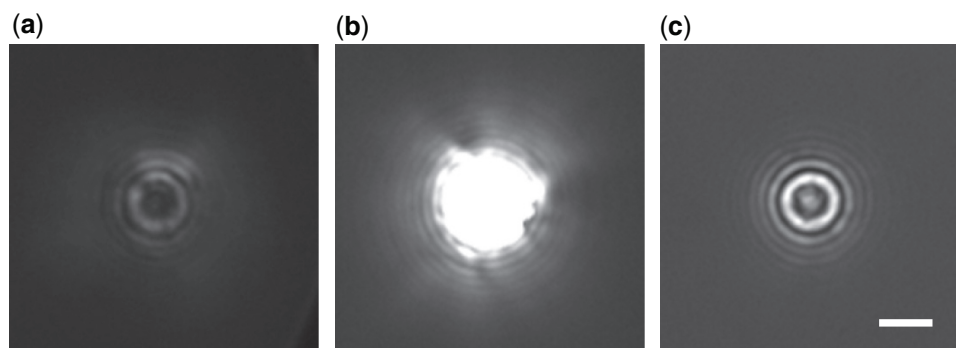


**Figure 3.** Interference images formed by reflected beams from the surfaces of (a) an uncoated bead and a coverglass, (b) a gold-coated bead and an uncoated coverglass and (c) a gold-coated bead and a dielectric coated coverglass. In image (b), the intensity of interference below the bead is saturated because of the high reflectance of the gold surface. The intensity in (c) is about 16 times higher than that of (a), and the contrast in (c) is  $\sim 60\%$  higher than that of (a). For the image in (c), a  $16\times$  neutral density filter is placed in the optical path of the incident illumination, which reduces background reflection intensity and prevents saturation of the CCD. Scale bar 2  $\mu\text{m}$  in (c).

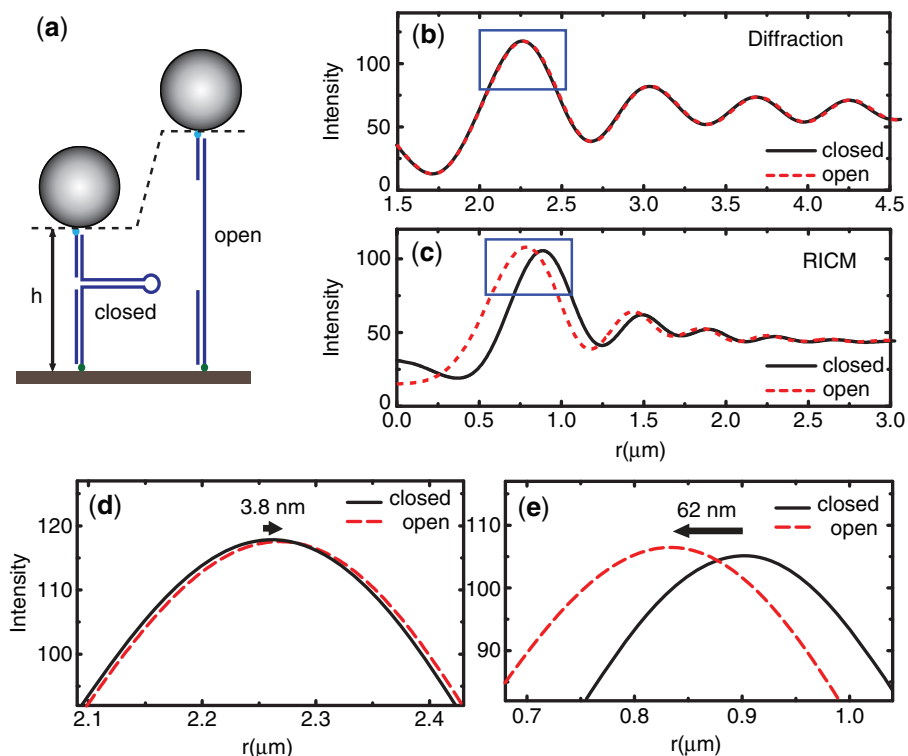


**Figure 4.** Comparison of diffraction- and RICM-based methods. (a) Schematic of DNA hairpin experiment. (b) Radial intensity profiles of diffraction patterns from a 2.8  $\mu\text{m}$  diameter bead. (c) Radial intensity profiles of reflected-interference patterns from a 4.5  $\mu\text{m}$  diameter bead. In (b) and (c), the solid (dashed) line corresponds to an intensity profile from the closed (open) state of the DNA hairpin S20T8; the boxed areas highlight the motion of the first fringe. (d) and (e) are magnifications of the boxed area in (b) and (c), respectively. In (b), the x-axis starts at 1.5  $\mu\text{m}$  to exclude the region in which the light is blocked by the sphere.

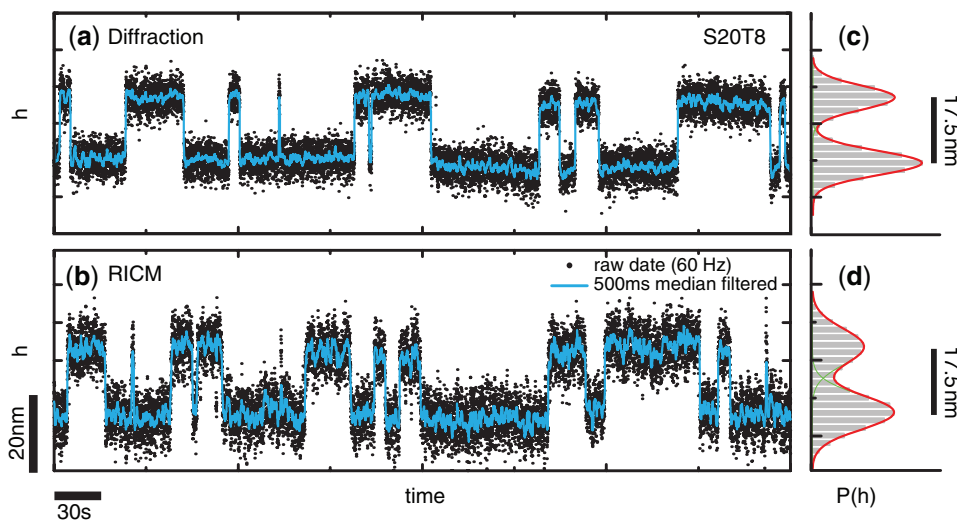


**Figure 5.** (a and b) Bead height versus time of a bead tethered by a dsDNA containing hairpin S20T8 measured at a constant applied force near the critical force using (a) diffraction from a 2.8  $\mu\text{m}$  diameter magnetic bead and (b) RICM from a gold-coated 4.5  $\mu\text{m}$  diameter magnetic bead. (c and d) Distributions of bead height calculated from the raw data in the (a) and (b), respectively.

indicating that our RICM calibration scheme is reliable. The RICM-based measurement shown in Figure 5b and d has a larger variance than that of the diffraction measurement (Figure 5a and c); this is not related to the instrumental resolution: basic fluctuation/dissipation arguments indicate that the larger bead size used here

for the RICM-based measurement leads to a larger predicted Brownian fluctuation (20), which dominates in the force regime used in this calibration experiment.

At constant applied force and tether length, smaller beads have less thermal noise; thus it is desirable to use smaller beads in the RICM measurement. The RICM

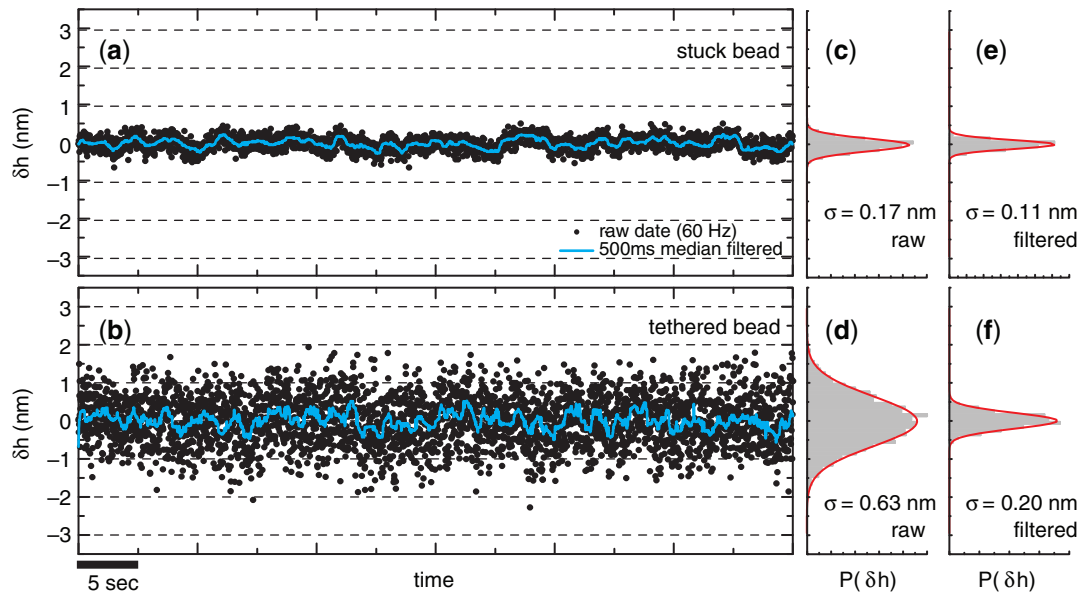


**Figure 6.** (a and b) Measured bead height versus time of (a) a bead immobilized on the coverglass and (b) a bead tethered to the coverglass by a 1738 bp dsDNA. Each data point was calculated from RICM data acquired with 8 ms exposure and 60 Hz frame rate (dots) and median filtered with a 500 ms window (solid lines). The force applied to the tethered bead is about 23 pN. (c–f) Histograms of bead height from the traces in (a) and (b); (c) and (d) are calculated using the 60 Hz raw data, while (e) and (f) are calculated using the median filtered data. The distributions are fitted by a Gaussian function (solid lines), with best-fit standard deviations shown.

strategy described here (i.e. the illumination and detection scheme and the height calibration method) can be applied to smaller beads without any changes in protocol. However, the RICM method requires a smooth bead surface to generate a clean interferogram; thus far, we have found only the Dynal 4.5  $\mu\text{m}$  diameter beads (and not the Dynal 1 or 2.8  $\mu\text{m}$  diameter beads) to have an adequately smooth surface. Future work is needed to either identify a manufacturer of small, smooth magnetic beads, or to fabricate them directly.

### Resolution test

We demonstrate the resolution of the RICM-based measurement by measuring the height of both a magnetic bead immobilized directly on the coverglass and a magnetic bead tethered by a single 1738-bp DNA molecule. Figure 6a shows a time trace of the apparent height of the immobilized bead in the absence of applied force. Using active stabilization, which uses a melted polystyrene bead as a reference mark (15), the focal position of the objective is maintained in the vicinity of the solution/coverglass interface. However, it is impossible for the focal position to be maintained in a perfectly stable fashion. Furthermore, non-specifically immobilized beads are known to undergo small motions (21). Thus, we attribute the fluctuations in Figure 6a to the imperfectness of both the active stabilization and the bead immobilization method. The data thus indicates that the instrumental resolution of RICM is below 0.2 nm in standard deviation (Figure 6c and e).

Figure 6b shows a time trace of the tethered bead subject to  $\sim 23$  pN of applied force. The corresponding standard deviation (Figure 6d and f) indicates the actual resolution: 0.62 nm at 8 ms exposure and 60 Hz frame rate,

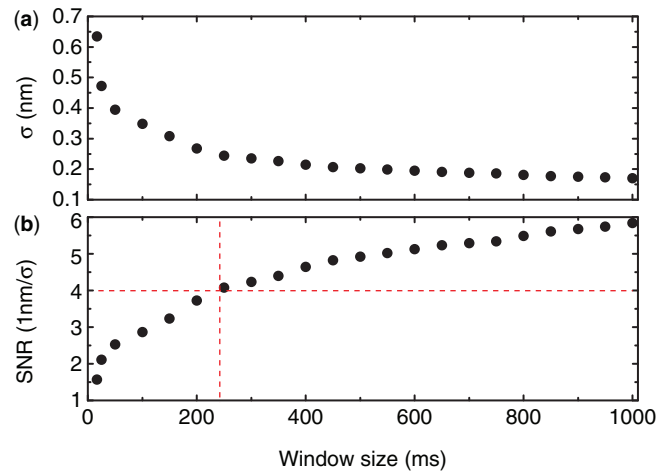


**Figure 7.** (a) Standard deviations of the time trace in Figure 6b as a function of the window size of the median filter. (b) SNR for a 1 nm step versus window size. The dashed line indicates the condition for which a 1 nm change in bead height can be resolved with an SNR of 4.

and 0.2 nm using a 500 ms window median filter. Here, the resolution is limited by the Brownian fluctuations allowed by the finite elasticity of the tether; they are well-accounted for by the Langevin theory (17), which predicts a standard deviation of  $0.61 \pm 0.05$  nm at 8 ms exposure.

When the applied force reduces the bead's Brownian fluctuations below 0.25 nm, we expect the RICM-based measurement can resolve sub-nanometer changes in bead height with a signal to noise ratio (SNR)  $>4$ . This is emphasized by the data in Figure 7a, which indicates the standard deviations of the trace in Figure 6b as a function of the window size of the median filter. In practice,

resolving step-like extension changes requires an SNR  $>4$  (22); furthermore, the choice of window size will be determined by the kinetics of the studied extension-changing process. Thus Figure 7b indicates that, for a 1738 bp tether under 23 pN of force, 1 nm steps can be resolved by RICM if they occur more slowly than  $\sim 225$  ms.

## CONCLUSIONS

We have demonstrated a high resolution MT based on RICM with a greater than 10-fold resolution increase over the traditional diffraction method. This improvement was enabled by the intrinsically higher sensitivity of the RICM fringes, the inclusion of thin films that enhanced the quality of the RICM interferograms, and the use of an active stabilization routine. We used a biomolecular calibration based on DNA hairpin unfolding to show that the RICM measurement of the length change is accurate. Our results show that the RICM-based MT system is well suited to precision measurements of configuration-changing biomolecular activity. We expect this system will provide a simple and powerful tool for the investigation of the physical properties of biological molecules.

## SUPPLEMENTARY DATA

Supplementary Data are available at NAR Online.

## ACKNOWLEDGEMENTS

The authors thank N. Ribbeck for comments.

## FUNDING

National Institutes of Health [grant number 1R21GM079584-01A1]. A portion of this work was done in the UCSB nanofabrication facility, part of the National Science Foundation funded National Nanotechnology Infrastructure Network. Funding for open access charge: National Institutes of Health [grant number 1R21GM079584-01A1].

*Conflict of interest statement.* None declared.

## REFERENCES

- Greenleaf, W.J., Woodside, M.T. and Block, M. (2007) High-resolution, single-molecule measurements of biomolecular motion. *Annu. Rev. Biophys. Biomol. Struct.*, **36**, 171–190.
- Neuman, K.C. and Nagy, A. (2008) Single-molecule force spectroscopy: optical tweezers, magnetic tweezers and atomic force microscopy. *Nat. Meth.*, **5**, 491–505.
- Lionnet, T., Dawid, A., Bigot, S., Barre, F.X., Saleh, O.A., Heslot, F., Allemand, J.F., Bensimon, D. and Croquette, V. (2006) DNA mechanics as a tool to probe helicase and translocase activity. *Nucleic Acids Res.*, **34**, 4232–4244.
- Strick, T.R., Allemand, J.F., Bensimon, D., Bensimon, A. and Croquette, V. (1996) The elasticity of a single supercoiled DNA molecule. *Science*, **271**, 1835–1837.
- van der Heijden, T., van Noort, J., van Leest, H., Kanaar, R., Wyman, C., Dekker, N.H. and Dekker, C. (2005) Torque-limited RecA polymerization on dsDNA. *Nucleic Acids Res.*, **33**, 2099–2105.
- Taneja, B., Schnurr, B., Slesarev, A., Marko, J.F. and Mondragón, A. (2007) Topoisomerase V relaxes supercoiled DNA by a constrained swiveling mechanism. *Proc. Natl Acad. Sci.*, **104**, 14670–14675.
- Lia, G., Semsey, S., Lewis, D.E., Adhya, S., Bensimon, D., Dunlap, D. and Finzi, L. (2008) The antiparallel loops in gal DNA. *Nucleic Acids Res.*, **36**, 4204–4210.
- Saleh, O., McIntosh, D., Pincus, P. and Ribbeck, N. (2009) Nonlinear low-force elasticity of single-stranded DNA molecules. *Phys. Rev. Lett.*, **102**, 068301.
- Gosse, C. and Croquette, V. (2002) Magnetic tweezers: micromanipulation and force measurement at the molecular level. *Biophys. J.*, **82**, 3314–3329.
- Ribbeck, N. and Saleh, O.A. (2008) Multiplexed single-molecule measurements with magnetic tweezers. *Rev. Sci. Instrum.*, **79**, 094301.
- Abbondanzieri, E.A., Greenleaf, W.J., Shaevitz, J.W., Landick, R. and Block, S.M. (2005) Direct observation of base-pair stepping by RNA polymerase. *Nature*, **438**, 460–465.
- Curtis, A.S.G. (1964) The mechanism of adhesion of cells to glass: a study by interference reflection microscopy. *J. Cell Biol.*, **20**, 199–215.
- Wiegand, G., Neumaier, K.R. and Sackmann, E. (1998) Microinterferometry: three-dimensional reconstruction of surface microtopography for thin-film and wetting studies by reflection interference contrast microscopy (RICM). *Appl. Opt.*, **37**, 6892–6905.
- Rädler, J. and Sackmann, E. (1993) Imaging optical thicknesses and separation distances of phospholipid vesicles at solid surfaces. *J. Phys. II France*, **3**, 727–748.
- Kim, K. and Saleh, O.A. (2008) Stabilizing method for reflection interference contrast microscopy. *Appl. Opt.*, **47**, 2070–2075.
- Gál, J., Schnell, R., Szekeres, S. and Kálmán, M. (1999) Directional cloning of native PCR products with preformed sticky ends (Autosticky PCR). *Mol. Gen. Genet.*, **260**, 569–573.
- Klaue, D. and Seidel, R. (2009) Torsional stiffness of single superparamagnetic microspheres in an external magnetic field. *Phys. Rev. Lett.*, **102**, 028302.
- Woodside, M.T., Behnke-Parks, W.M., Larizadeh, K., Travers, K., Herschlag, D. and Block, S.M. (2006) Nanomechanical measurements of the sequence-dependent folding landscapes of single nucleic acid hairpins. *Proc. Natl Acad. Sci.*, **103**, 6190–6195.
- Smith, S.B., Cui, Y. and Bustamante, C. (1996) Overstretching B-DNA: the elastic response of individual double-stranded and single-stranded DNA molecules. *Science*, **271**, 795–799.
- Gittes, F. and Schmidt, C.F. (1998) Thermal noise limitations on micromechanical experiments. *Eur. Biophys. J.*, **27**, 75–81.
- Carter, A.R., King, G.M., Ulrich, T.A., Halsey, W., Alchenberger, D. and Perkins, T.T. (2007) Stabilization of an optical microscope to 0.1 nm in three dimensions. *Appl. Opt.*, **46**, 421–427.
- Wallin, A.E., Salmi, A. and Tuma, R. (2007) Step length measurement – theory and simulation for tethered bead constant-force single molecule assay. *Biophys. J.*, **93**, 795–805.